NUKLEONIKA 2006;51(1):15–20

INVITED PAPER

Development of diagnostic tools for Plasma Focus derived X-ray source

**Ergisto Angeli,
Claudio Bonifazzi,
Andrea Da Re,
Michele Marziani,
Agostino Tartari,
Michele Frignani,
Simone Mannucci,
Domiziano Mostacci,
Federico Rocchi,
Marco Sumini**

Abstract The energy spectra of X-rays generated by the impact of electron beams on high- and medium-Z targets following the pinch implosion of Plasma Focus (PF) devices are discussed in terms of the possible mechanisms of X-ray production following electron impact ionization. In addition, the temperature measurement of the PF inner electrode is reported and some results have been proved useful in order to optimize the device functionalities.

Key words plasma focus • electron impact ionization • characteristic X-ray lines • bremsstrahlung • material heating • dosimetry

E. Angeli, A. Da Re, M. Marziani, A. Tartari✉
Department of Physics,
University of Ferrara,
1 Saragat Str., I-44100 Ferrara, Italy
and INFM, Genova, Italy,
Tel.: +39 0532 974211, Fax: +39 0532 974210,
E-mail: tartari@fe.infn.it

C. Bonifazzi
Department of Biomedical Sciences,
University of Ferrara,
17/19 Fossato di Mortara Str., I-44100 Ferrara, Italy

M. Frignani, S. Mannucci, D. Mostacci,
F. Rocchi, M. Sumini
Laboratory of Nuclear Engineering of Montecuccolino,
University of Bologna,
16 dei Colli Str., 40136 Bologna, Italy
and INFM, Genova, Italy

Received: 25 August 2005
Accepted: 15 December 2005

Introduction

Plasma Focus (PF) derived X-ray sources may find potential applications in medicine and industry [4]. It represents a solution at low cost of management, is compact and reliable and offers performances in terms of intensity and of the time of exposure (< 100 ns). The main peculiarity of the PF radiation is represented by a very intense beam and short exposure time together with a strong electromagnetic radio frequency production. So, the usual diagnostics based on wavelength dispersive device or large arrays of NaI and silicon PIN detectors are not suitable because of the high electromagnetic noise. Following the procedure similar to that utilized for X-ray spectrometry from terawatt laser sources an X-ray spectrometric measurement was carried out by means of a differential absorption technique based on calibrated LiF TLD dosimeters which allow a measurement of an attenuation curve at a given time [10]. The energy distribution of the produced X-rays is then calculated, from such attenuation data, using an iterative procedure based on spectral algebra formalism. A systematic comparison of different X-ray beams observed at different PF exit windows is carried out and discussed in terms of the possible mechanisms of X-ray production following electron impact ionization.

In addition, in order to have devices industrially competitive, Plasma Focus needs to be operated in the so-called repetitive mode. However, at each pulse, or shot, part of the machine input energy is converted into thermal loads on the structural components of the machine itself, and this can be a major cause for the mechanical failure of a device operated in repetitive mode. The amount of energy converted into heat at

each shot needs to be known in order to design efficient cooling apparatuses. Unfortunately, no quantitative data about PF heating have ever been published so far. In this paper, the results of an experimental campaign, aimed at estimating the heat generated in the inner electrode of a PF, are presented for the first time and compared with theoretical models. These results will be of help in the design of the cooling systems needed for the repetitive operation of PF.

Material and methods

The Plasma Focus device and X-ray diagnostics

The experimental set-up is shown in Fig. 1. The Plasma Focus is a Mather-type device with a hollow inner anode that allows piping of the back-warded electron beam. The energy of the capacitor bank is 7 kJ with a maximum peak current of 0.5 MA at a working voltage of 17.0 kV. In the present paper, we consider only the X-ray production due to the impact of: (a) electron beams turning back to the inner electrode after the implosion of the current sheet into the pinch, and (b) relativistic electron beams (REB) originated in the pinch zone and backward accelerated in a narrow cone along the axis of the electrodes. In the case of X-ray characterization the PF was operated at a fixed atmosphere of 6.0 torr of H_2.

The X-ray characterization is performed by extracting the photon beams through four windows positioned around the pinch region. One of them, forward positioned and aligned with the electrodes axis, looks at both the pinch and the portion of electrode interested to the impact of turning-back electrons. Other two windows are positioned laterally to the pinch region and look at the same region as the preceding one. All these windows are equipped with double-layered sheets composed of 24 μm thick aluminised Mylar plus 18 μm thick aluminium foils; these are used to suppress the soft X-ray component directly produced in the pinch region, i.e. photons with energy $E < 3$–4 keV.

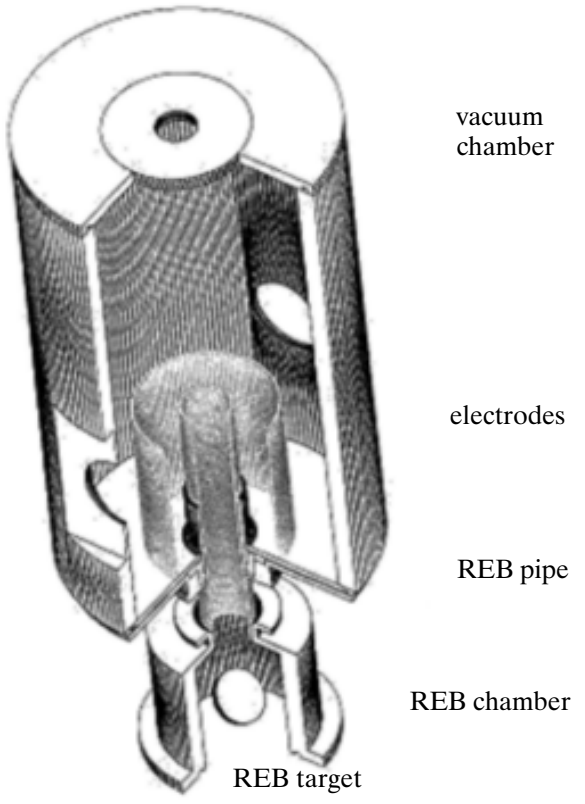

Fig. 1. Sketch of the experimental apparatus based on Plasma Focus discharges.

For the measurement of the REB based X-ray source, a special chamber to be fixed at the end of the inner electrode has been constructed. A target holder, well collimated to the REB and to the spectrometer window, is positioned inside this chamber. The target is 45° tilted with respect to the electrodes axis and is placed at about 10 cm from the beginning of the anode.

The spectrum of the X-rays is evaluated using a differential absorption based technique [9]. The X-ray spectrometer consists of a stack of LiF dosimeters which act both as detectors and filters to give curves of attenuated intensities. The energy distribution is calculated from such attenuation curves using an iterative procedure based on spectral algebra formalism. The LiF dosimeter nearest to the source acts at the same time as exposure meter.

Relationship between thermoluminescent counts and photon intensity

The dosimeters are calibrated at the well established 59.54 keV X-ray facility of the Department of Physics, University of Ferrara which utilizes a 1.85×10^{10} Bq ^{241}Am sealed source emitting 2.8 E08 photons/s/sr. Taking into account that the number of thermoluminescence counts is induced by the whole energy deposition into the dosimeter and, referring to a planar geometry in which the dosimeter surface is normal to the direction of the photon beam, we can define the absorbed energy rate per solid angle:

$$E_A = I(E)\left(\frac{\mu_{en}(E)}{\rho}\right)Et_D \qquad (1)$$

where $I(E)$ is the number of photons per second and solid angle of the beam and t_D is the crossed thickness of the dosimeter. $\mu_{en}(E)/\rho$ (with ρ the density of LiF material) is the energy absorption coefficient of LiF as defined by Hubbell and Seltzer 1995 [6]. Bearing in mind that the thermoluminescence is induced by the whole energy deposition E_A into the dosimeter, in the case of a monochromatic beam of photon energy E the resulting thermoluminescent counts will be given by means of the response factor $K(E)$, i.e. $c = K(E)E_A$.

The essential independence of the LiF response over energy [5] allows the absorbed energy to produce the thermoluminescent count c which is the same regardless of the energy of the incident photon. This leads to the definition of a conversion factor F_c to compare thermoluminescent counts at different energy E of the photon beam and irradiation geometry (solid angle Ω) with the following relationship:

$$(2) \qquad I(E) = c_M \frac{I(E_c)\left(\frac{\mu_{en}(E_c)}{\rho}\right)E_c\Omega}{c_c\left(\frac{\mu_{en}(E)}{\rho}\right)E\Omega_M}$$

i.e. $I(E) = cF_c(E)$.

In equation (2), the index "c" and "M" refer to the calibration with monochromatic photons and actual measurement with PF beams, respectively.

Moreover, the assumption of the dosimeter energy response independence leads to the validation of the energy photon hardening evaluation by successive attenuation of staked TLD dosimeters which form the basis of differential absorption spectrometry.

For a polychromatic beam, the energy transmission $T_M(t)$ after passing the thickness t of material is:

$$(3) \qquad T_M(t) = \frac{\int_0^{E_{\max}} I(E)\mu_{en}(E)Ee^{-\mu(E)t}dE}{\int_0^{E_{\max}} I(E)\mu_{en}(E)EdE}$$

Being the denominator a constant (k), defined by the measurement of the first vicinal detectors, it follows that by choosing n measurements (with t_1,..., t_n thickness), and dividing the energy interval into n bins (with E_1,.., E_n energies) the relationship between the measured transmission series $T_M(t_i)$ and the energy spectrum of the incident beam can be expressed in terms of matrix formalism as:

$$(4) \qquad \begin{bmatrix} T_M(t_1) \\ \dots \\ T_M(t_n) \end{bmatrix} = \frac{1}{k}\begin{bmatrix} A(E_1,t_1),\dots,A(E_n,t_1) \\ \dots \quad \dots \quad \dots \\ A(E_1,t_n),\dots,A(E_n,t_n) \end{bmatrix} \cdot \begin{bmatrix} I(E_1) \\ \dots \\ I(E_n) \end{bmatrix}$$

where:

$$(5) \qquad A(E_i,t_i) = \mu_{en}(E_i)E_i e^{-\mu(E_i)t_i}q_i$$

In equation (4), T_M refers to the transmission measurement, i.e. the ratio between the actual reading of the *i-th* dosimeter and that of the first one which represents the un-attenuated measurement. μ_i is the attenuation coefficient at energy E_i of the LiF material. As can be seen in Eq. (5), all terms are independent of the energy spectra and can be obtained from the usual data bases [6].

Temperature measurement

Temperature measurements were performed with a type *K* thermocouple which was kept fixed in the position of direct contact with the inner surface of the inner electrode by a very small aluminium ring spring. The thermocouple tip was positioned at about 4.5 cm from the end of the electrode.

The data readout was made with a data logger which could send data to a PC via RS232 connection. The uncertainty in temperature measurement was ± 0.5°C, so that only values differing by 1°C could be obtained. The sampling frequency was 0.2 Hz; higher frequencies resulted in a data redundancy which proved to be, once tried, an obstacle in the analyses of data.

In this experimentation, the plasma focus was operated at 6, 8, 10 or 12 torr of D_2. For each shot, the total current and the total neutron yield were measured with a Rogowski coil and a silver activation counter, respectively [11].

The temperature decay modelling is performed by means of the well known Newton law:

$$(6) \qquad T(t) = T_A + \Delta Te^{-kt}$$

with T_A being the initial environment temperature before PF firing and ΔT the temperature increase after a given shot. "k" is a positive parameter which describes altogether all the possible different cooling mechanisms (conduction, convection and radiative transfer) which are very difficult to separate and distinguish also via theoretical simulation.

The heat loading is consequently determined by

$$(7) \qquad Q = m_f c_p \Delta T$$

with m_f being the fraction of the mass actually heated and c_p the specific heat of the material composing the observed part.

Results and discussion

X-ray production

The quantities in the second member of Eq. (1) and their energy dependence will affect the conversion factor when different photon energy is concerned. In Table 1, the estimation of such quantities are reported. Corresponding quantities are reported in Table 2 for the PF measurements. With the values of Tables 1 and 2, the conversion factor F_c results in 4.87 E09 photons/counts/sr, the fluence at the pinch source being equal to 9.7 E14 photons/shot/sr, if the window attenuation is not accounted. With the attenuation accounted and hypothesizing a photon energy of 25 keV, the fluence at the pinch position will be 5.0 E15 photons/shot/sr.

Table 1. Quantities involved in the calibration procedure

Photon energy E_c	59.54 keV (9.53 E-15 J)
Dosimeter (LiF) density	2.64 g/cm^3
Dosimeter dimension	(0.3 × 0.3 × 0.1) cm
Dosimeter mass (estimated)	2.4 E-02 g
Dosimeter mass (measurements)	(2.4 E-02 ± 1.5 E-04) g
$I(E)$ flux at the source	2.8 E08 photons/s/sr
Exposure time	3600 s
Thermoluminescent counts c_c	9100
Solid angle Ω_c	0.094 sr
$\mu_{en}(E_c)/\rho$ at 59.54 keV	3.22 E-02 cm^2/g

Table 2. Quantities involved in the PF measurements with 100 μm Cu window cut off (≈ 21 keV)

Energy E (hypothesized)	25 keV
Source – dosimeter distance	150 mm
$\mu_{en}(E)/\rho$ at 25.0 keV	0.41 cm^2/g
Solid angle (estimated)	4 E-04 sr
Exposure time	50.0 E-09 s
Thermoluminescent counts	1.0 E03
Cu window thickness	100 μm
Window transmission at 25 keV	0.212

Table 3. Comparison with other sources

Source	Energy, keV	Fluence/sr (at source position)
^{241}Am 1.85×10^{10} Bq	59.54	2.8 E08 photons/sr/s
X-ray tube	56.5	6.1 E14 photons/sr/s
X-ray tube	17.9	5.6 E13 photons/sr/s
PF-REB single shots	25.0	5.0 E15 photons/sr/shot

In Table 3, a comparison with other photon sources is made on the basis of data taken from HPA 1979 Catalogue [1] in the case of X-ray tubes. Such data, together with those of REB PF source, are scaled to the geometrical condition of the ^{241}Am facility geometry. At a first sight, the PF source looks very similar to that given by the ordinary diagnostic X-ray tubes. However, such intensity is not referred to 1 s unit time, as for X-ray tubes or sealed radioisotopes, but is delivered in about 30–50 E-9 seconds.

An example of the energy spectra calculated by means of the above mentioned formalism from the measured attenuation curves is shown in Fig. 2 for the two modalities of X-ray production by electron impact, i.e. the brass target material for the lateral exit window and a tungsten target material in case of the REB. The results show that the energy spectra of the photons consist mainly of characteristic L X-rays in case of high-Z materials like tungsten and K X-rays for low or medium-Z materials like zinc and copper forming the considered brass alloy. This characteristic radiation is superimposed to a continuous low intensity bremsstrahlung whose photon energy extends up to several tens of keV. Figure 3 shows a comparison between the normalized attenuation curves in the case of a brass REB target similar in composition to the inner anode material. As can be noted, the REB component seems to exhibit an electron energy higher than those impinging on the inner anode. This conclusion partially supports the results of Bostik *et al.* [2] about the presence in the REB of high energy components by using a device very similar to the present one [8].

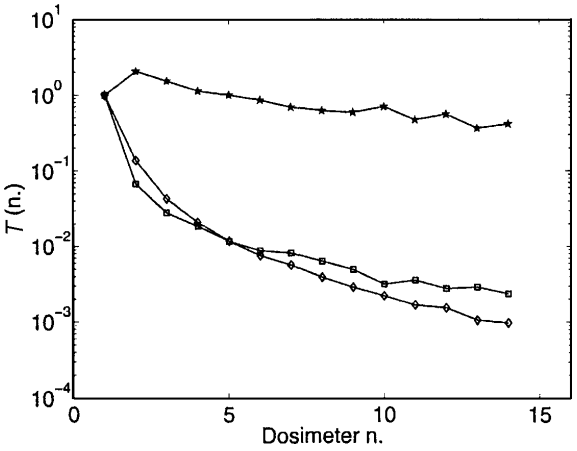

Fig. 3. Transmission curve for different quality of X-ray beams. ∗ – lateral/REB ratio; □ – REB; ◊ – lateral direction.

Using the well-known EGS4 Monte Carlo code modified to include the characteristic X-rays production by electron impact [3, 8], the spectra of the emitted photons from an energetic electron beam against a high-Z target may be simulated and the results compared with those given by the spectrometer assessment. An example of these spectra is shown in Fig. 4 for a tungsten target REB impact with energy of 50 keV. In these simulated spectra, two components, the characteristic radiation and the continuous bremsstrahlung can be seen in a similar look as those of Fig. 2. The Monte

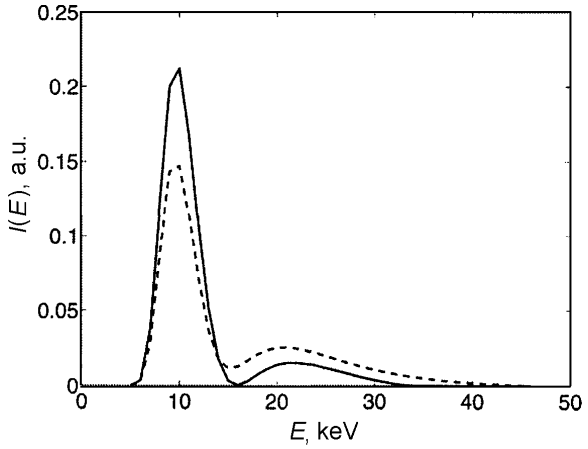

Fig. 2. Calculated energy spectra of the X-rays measured in the REB window (dotted line) and in the lateral window (continuous line).

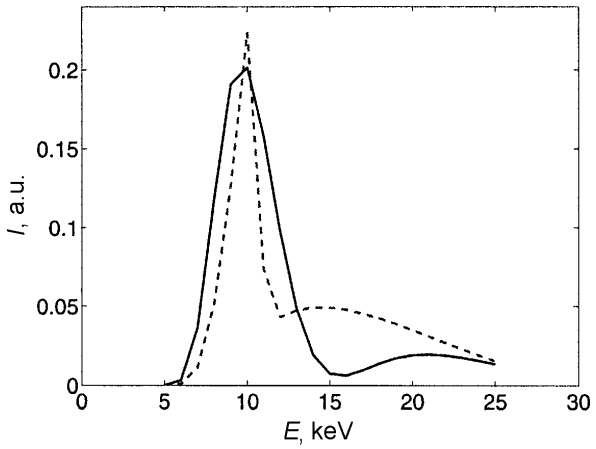

Fig. 4. Comparison of EGS4 Monte Carlo simulation, dotted line, and the experimental measured spectra, continuous line.

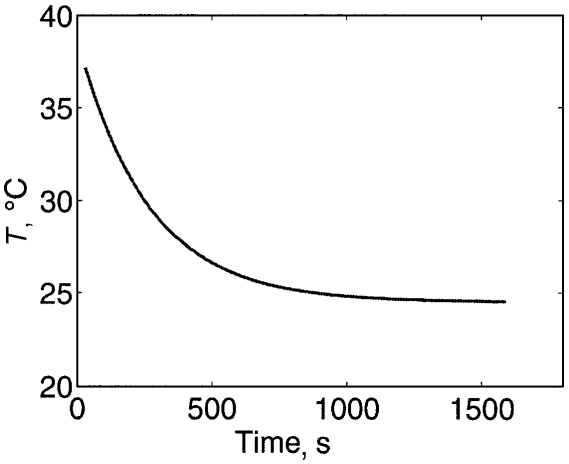

Fig. 5. Measurement of the temperature decay of the inner electrode (anode) after a shot.

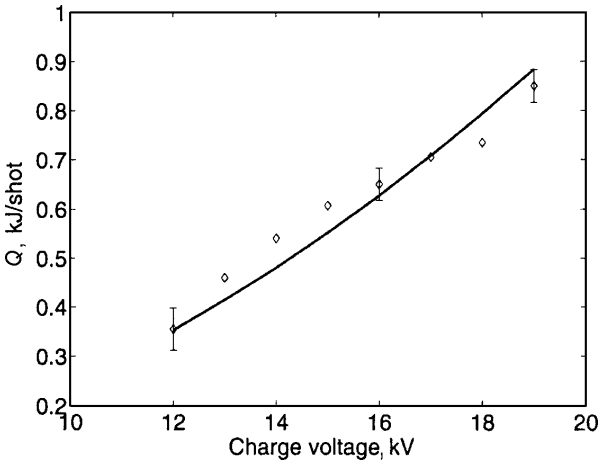

Fig. 6. Charge voltage dependence of the heat load at 8 torr of D_2 filling atmosphere. ◊ – experimental; —— – $Q = 0.00245(V)^2$ interpolation curve.

Carlo results are far to be in good agreement with experimental data especially in regard to the experimentally observed huge enlargement of the characteristic L X-ray line group. This enlargement is well beyond the estimated spectrometer resolution which is conservatively included in the EGS4 results presented in Fig. 4. One hypothesis is to consider phenomena like that induced by multiple ionization followed by satellite line in the K and L lines spectra [7]. This possibility together with the inclusion of a failure in the inversion algorithm of Eq. (4), forms the actual work in progress.

Heat load measurements

An example of the inner electrode temperature time decay after a shot at 19 kV is given in Fig. 5. The evaluated ΔT for this series was 17.19°C and the coefficient k was found to be 0.003803 s^{-1}.

It has been found a rather strong dependence of ΔT on the bank energy, as it might be expected. Therefore, for each integer value of the voltage in kilovolts from 12 to 19 kV at least 10 series of either 5 or 10 shots were done and the relative ΔTs were evaluated. Figure 6 shows the variation against bank charge voltage of the inner electrode thermal deposition per shot. The dependence is found to follow a power law estimated as $Q = 0.00245(V)^2$ with Q in kJ and V in kV. This leads to conclude that a linear dependence with the bank energy ($E = 0.5CV^2$ with C the total bank capacitors) may be accepted. It must be said that all the points shown were obtained from a series of shots performed at the same pressure of 8 torr (the present PF neutron production is optimized at this pressure for 7 kJ bank energy); nonetheless no sensible variation of these results with pressure has been found.

Operation at different values of pressure (6, 8, 10 or 12 torr) gave the same results. Moreover, the formation of a good pinch does not imply higher heating; discharges in which no pinch at all was seen provided the electrode with the same amount of heat as those in which a very good pinch was obtained. These two observations are in agreement with the fact that the total neutron yield does not influence (nor is somehow correlated with) the heating of the electrode. Moreover, a series of discharges with a good neutron yield heated the electrode in the same way of series with a low neutron yield. The unique requisite for a consistent heating is simply the formation of the plasma sheath. The decision to have a massive inner electrode (so to have higher heat capacity) or a thin hollow electrode with a heat removal system must be taken, therefore with great care.

Acknowledgment This work was partially supported by MIUR, Rome, Italy and INFM, Genova, Italy.

References

1. Birch R, Marshall B, Ardran GM (1979) Catalogue of spectral data for diagnostic X-rays. HPA, London, SRS 30
2. Bostik WH, Nardi V, Prior W *et al.* (1983) Production of GW electron and ion beams by focused discharges. In: Nardi V, Salin H, Bostik WH (eds) Energy storage, compression and switching. Plenum Press, New York, pp 267–287
3. Casnati E, Tartari A, Baraldi C (1982) An empirical approach to *K*-shell ionization cross section by electrons. J Phys B-At Mol Opt 15:155–167
4. Gribkov VA (2000) On possible formulation of problems of a dense Plasma Focus used in material science. Nukleonika 43;3:149–153
5. Horowitz YS, Kalef-Ezra J (1981) Relative thermoluminescent response of LiF TLD. Nucl Instrum Meth 188:603–607
6. Hubbell JH, Seltzer SM (1995) Tables of X-ray mass attenuation coefficients and mass energy absorption coefficients 1 keV to 20 MeV for elements Z = 1 to 92 and 48 additional substances of dosimetric interest. NSTIR 5632, Gaithersburg MD, USA
7. Jacobs VL, Davis J, Balazs SF, Cooper JW (1980) Multiple ionization and X-ray emission accompanying the cascade decay of inner shell vacancies in Fe. Phys Rev A 21:1917–1926
8. Marziani M, Gambaccini M, Tavora L, Taibi A (2001) Monte Carlo simulation of mammography X-ray units: a comparison between different electron extensions of the EGS4 code system. In: Khing A, Barão F, Nakagawa N, Tavora L, Vaz P (eds) Advances Monte Carlo for

radiation physics, particle transport simulation and applications. Springer-Verlag, Berlin, pp 351–356
9. Schnuerer M, Nolte R, Sclegel T *et al*. (1997) On the distribution of hot electrons produced in short pulse laser plasma interaction. J Phys B-At Mol Opt 30:4653–4661
10. Tartari A, Da Re A, Bonifazzi C, Marziani M (2004) Energy spectra measurements of X-ray emission from electron interaction in a dense Plasma Focus device. Nucl Instrum Meth B 213:206–209
11. Tartari A, Verri G, Da Re A, Mezzetti F, Bonifazzi C, Rapezzi L (2002) Improvement of calibration assessment for gold fast neutron activation analysis using Plasma Focus devices. Meas Sci Technol 13:939–945